

An Investigation into the Origin of Autopoiesis

Randall D. Beer*

Indiana University
Cognitive Science Program
rdbeer@indiana.edu

Abstract Using a glider in the Game of Life cellular automaton as a toy model of minimal persistent individuals, this article explores how questions regarding the origin of life might be approached from the perspective of autopoiesis. Specifically, I examine how the density of gliders evolves over time from random initial conditions and then develop a statistical mechanics of gliders that explains this time evolution in terms of the processes of glider creation, persistence, and destruction that underlie it.

Keywords

Autopoiesis, origin of life, statistical mechanics, cellular automata

I Introduction

The origin of life remains one of the most fascinating and frustrating puzzles in science [23, 29, 36]. Not only is it a singular event in our own history, but it engages some of the most fundamental and potentially universal questions in biology. For example, any discussion of the origins of life necessarily involves taking a stance, either explicitly or implicitly, on the difficult problem of what life is in the first place. If one equates a living system with its molecular components, then the question of origins becomes one of biochemistry: What reactions gave rise to the particular set of biomolecules that underlie terrestrial life? In contrast, if one identifies life with its potential for evolution, then concern shifts to the origin of replication. From an energetic perspective, the problem is how metabolic cycles arose to harness energy flows. If one conceives of the essence of living systems as informational, then the origin of the genetic code becomes a central focus. And so on.

Terrestrial life consists of a complicated set of intertwined biochemical processes of metabolism, compartmentalization, and replication. Unfortunately, its modern form provides little direct evidence for the historical pathway by which life emerged from its abiotic precursors. In origin-of-life debates, the main battle lines are usually drawn between replication-first and metabolism-first scenarios, although compartmentalization is also frequently mentioned [22]. In the replication-first scenario, life began as a self-copying molecule. By far the most common version of this idea is currently the RNA world hypothesis, in which it is argued that because RNA molecules can play both informational and catalytic roles, they preceded and enabled the later adoption of DNA for template-based replication and proteins for catalysis [18]. In contrast, in the metabolism-first scenario, life began with autocatalytic networks of chemical reactions that were able to sustain their organization under far-from-equilibrium conditions by dissipating available flows of energy [15, 19]. Finally, compartmentalization emphasizes the need for any biochemical machinery to be contained within membranes that maintain their cohesion, protect them from disruptive external influences, and regulate the necessary exchange of waste and nutrients with the external environment [28, 30].

* Corresponding author.

One conception of life that has played little direct role in investigations into its origins is Maturana and Varela's notion of autopoiesis [25, 34]. Broadly speaking, autopoiesis falls into the general class of contained metabolism conceptions of life. However, it is formulated at a much more abstract level of description. Autopoiesis attempts to characterize living systems in a way that abstracts away the specific biochemical details of terrestrial life and the many secondary features it exhibits that are often taken as definitional. Instead, Maturana and Varela sought to highlight only universal principles, which they conceived as fundamentally organizational in nature. Specifically, an autopoietic (*lit.* self-creating) system is a network of processes that have the dual properties of self-production and self-individuation. Self-production means that the network of processes produces components whose interactions generate and maintain the very same network of processes that produced them. Self-individuation means that the system constructs and maintains its own boundary as an essential part of its operation. In Maturana and Varela's terms, a living system is an autopoietic system operating in the physical world (i.e., a molecular autopoietic system).

What might an analysis of the origin of life look like from the perspective of autopoiesis? Given its abstract character, autopoiesis obviously has nothing specific to say about the energetic favorability of one biochemical pathway over another. Likewise, it has little to say about the origin of replication, since autopoiesis is more concerned with the problem of persistence of the individual and views reproduction as an additional complication. On an autopoietic account, life begins when autopoiesis begins, by whatever process. Thus, questions about the origin of life in some particular universe become questions about the origin of autopoiesis in that universe. As a first step in the investigation of such questions, we adopt a statistical treatment. Since a given autopoietic organization defines a set of possible structural instantiations, we can examine the statistical mechanics of those configurations by coarse-graining over individual components and processes. Of particular interest are the processes that create, preserve, and destroy those configurations.

Previous work has utilized Conway's Game-of-Life (GoL) cellular automaton as a simple model within which to carry out a systematic theoretical exploration of the concept of autopoiesis and its consequences [4]. The basic idea was to treat GoL as a kind of physics from which we can derive an artificial chemistry. Bounded persistent spatiotemporal entities such as gliders were then analyzed in terms of the network of reactions that underlie them, and these networks were shown to satisfy an interpretation of the self-production and self-individuation conditions [6]. The interaction between such individuals and their environments was also characterized [5]. The only specific result from this previous work that I needed for the present article was that the resulting glider organization admits, at each grid location, the 16 structural instantiations shown in Figure 1 (2 forms \times 2 chiralities \times 4 orientations). My investigation was formulated entirely in terms of the statistical mechanics of sets of these configurations.

The goal of this article was to extend this research program to an exploration of questions on the origin of life from an autopoietic perspective, using a glider in the Game of Life as a toy model. Specifically, I developed a statistical mechanics of gliders and used it to study their origin, proliferation, and extinction. It is important to be as clear as possible about the purpose and limitations of this investigation. GoL provides a simple model universe in which we can study in detail the transition to autopoietic entities. Such models can help to hone our intuitions and to develop the conceptual, mathematical, and computational tools necessary to move forward. A consideration of the possible implications of this investigation for the origin of life in the physical universe will be left for the discussion section at the end of the article.

The article is organized as follows. I begin with a brief review of the general statistical properties of GoL. This is followed by a large simulation experiment examining how the density of gliders evolves over time from random initial conditions parameterized by the initial 1-density (the number of ones per site). I then develop a theoretical framework for studying the statistical mechanics of gliders and the processes of creation, persistence, and destruction that underlie their time evolution. This framework is then used to explain the main features of the simulation experiment. After showing how the basic theoretical framework can be extended to calculate more refined properties, the article concludes with a discussion of some possible implications for thinking about the origin of biological life and directions for future work.

An earlier version of this article appeared previously [8].

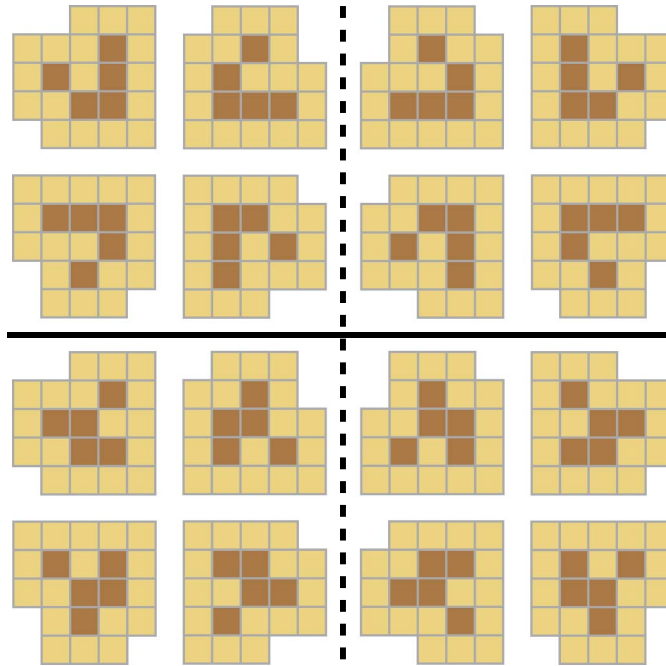


Figure 1. The 16 possible configurations of a glider in the Game of Life. The horizontal black line separates the wedge (top) and rocket (bottom) forms. The dashed vertical gray line separates the left- and right-handed configurations. Each quadrant contains the four possible orientations of a configuration with a given form and chirality.

2 Some Facts of Life

The general statistical evolution of the GoL universe provides the background against which the emergence, proliferation, and extinction of gliders occur. Gliders both contribute to and are influenced by that evolution. Accordingly, I begin with a brief review of the mean density evolution of GoL from random initial conditions [3, 27].

Consider a 100×100 grid with periodic boundary conditions. At time $t = 0$, we randomly initialize the grid by setting each site to 1 with a probability p (0 with a probability $1 - p$). The initial 1-density in a grid whose states are chosen in this way will be binomially distributed, with a mean of p and a variance of $p(1 - p)$. We then evolve the grid forward in time using GoL physics, and track its density. Repeating this experiment many times gives an estimate of the mean density evolution of GoL, $\bar{\rho}_t(p)$.

There is a strong general tendency for the mean 1-density to decay toward 0 over time regardless of its initial value. For a wide range of initial densities $0.15 \leq p \leq 0.6$, this decay exhibits a universal form divided into three epochs (Figure 2(a)). First, there is an initial transient whose shape and duration depend on p . Second, there is a power law decay with a scaling exponent of $\beta \approx -0.36$ (dotted line). Finally, the power law decay flattens out to a common asymptotic density of $\bar{\rho}_\infty \approx 0.029$ (dashed horizontal line).

The general long-term behavior of GoL is perhaps best illustrated by plotting an estimate of its asymptotic 1-density as a function of p (Figure 2(b)). In this plot, the behavior described above shows up as a large flat region of nonzero $\bar{\rho}_\infty$. Sufficiently far outside of this range, we observe very different behavior, with the 1-density falling all the way to 0. Between these two regions of distinct $\bar{\rho}_\infty$ values are transition regions in which $\bar{\rho}_\infty$ varies smoothly with p . Thus, gliders exist in a universe in which the mean 1-density is generally falling over time and whose long-term fate depends only weakly on p except for two transition regions centered around $p \approx 0.065$ and $p \approx 0.757$.

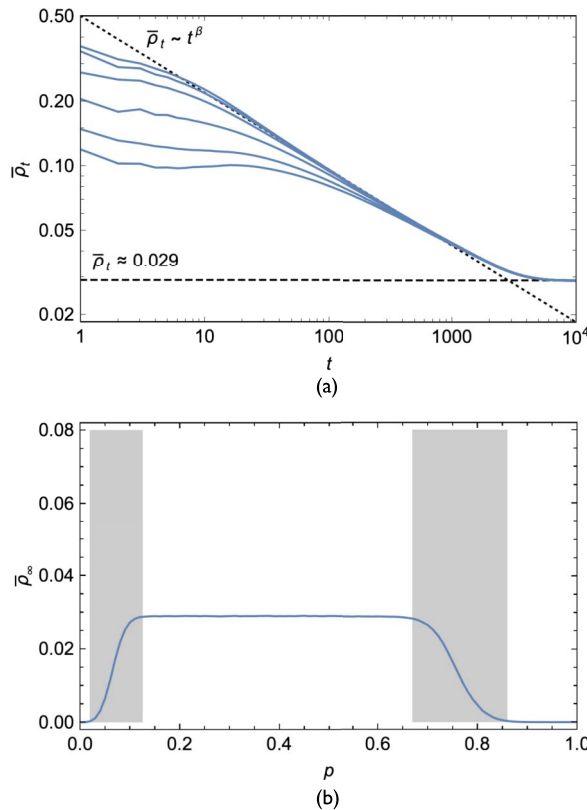


Figure 2. The time evolution of mean density in GoL. (a) A log-log plot of the time evolution of mean l-density $\bar{\rho}_t(p)$ for different initial l-probabilities $p = 0.15, 0.2, 0.3, 0.4, 0.5, 0.6$. (b) The asymptotic mean l-density $\bar{\rho}_\infty(p)$ as a function of l-probability p , with transition regions marked in gray. All curves represent the mean of 10^5 samples.

3 Mean Glider Density Evolution

We now turn our attention to the time evolution of the mean glider density. Let us begin with some data. We duplicate the experiment described in the previous section, except now we track mean glider density rather than l-density. Repeating this experiment many times over a fine grid of l-probabilities gives us a map of the time evolution of the mean glider density as a function of p (Figure 3(a)).

This map reveals several interesting features. Gliders generally exist over only a limited range of initial l-probabilities and time, which we might call the glider era. For $0.2 \leq p \leq 0.6$, the mean glider density rises very quickly to a peak at $t \approx 60$ and then begins a slow fall toward 0. However, as we approach the lower value of $p \approx 0.04$ or the upper value of $p \approx 0.85$, the pattern changes. Now there is a delay before the increase begins and a much slower rise toward a lower peak. Interestingly, near these transition regions, the population of gliders never quite decays to 0 (dim horizontal bands in Figure 3(a)). At still more extreme values of p , gliders never arise.

Some of this structure can be seen more clearly in high-resolution slices at constant p or t (Figure 3(b), 3(c)). At $t = 0$, the mean glider density has a single peak at $p \approx 0.23$. By $t = 5$, a burst of glider creation at larger p values has produced a second peak at $p \approx 0.64$. Subsequent glider creation at intermediate p values then lifts the valley between these two peaks until, by $t = 60$, a broad mesa appears. This mesa then begins to slowly decrease in height over the next several thousand time steps until its center collapses by $t = 5000$, leaving behind two small peaks at its edges corresponding to the two faint bands of glider persistence mentioned earlier.

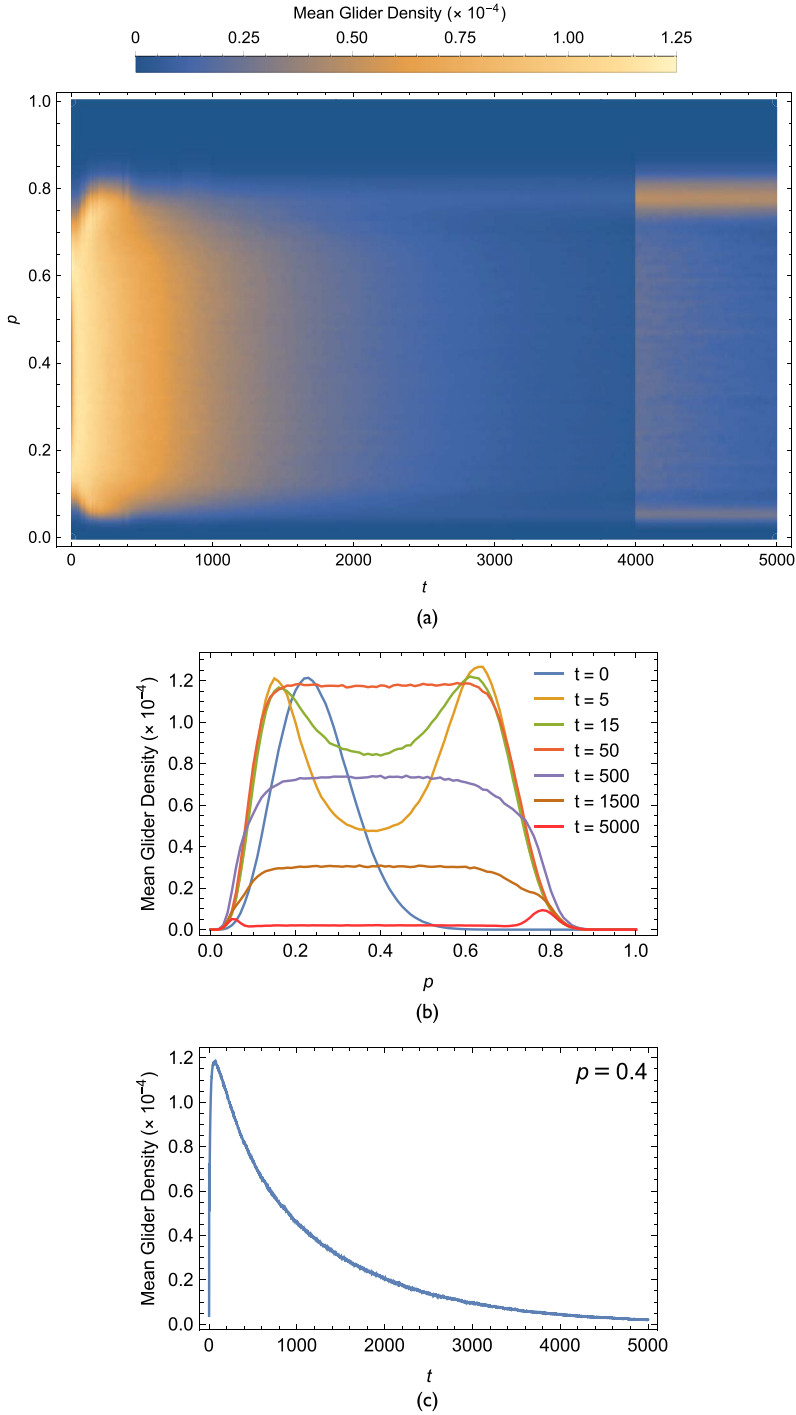


Figure 3. An experimental study of the time evolution of gliders. (a) Mean glider density $\bar{g}_t(p)$ as a function of time t and initial l-probability p . For each value of p (resolution $\Delta p = 0.01$), the corresponding strip of time (resolution $\Delta t = 1$) represents the time evolution of the mean glider density for 10^4 random initial conditions on a 100×100 grid with periodic boundary conditions. The portion of the plot for which $t > 4000$ has been scaled by a factor of 5 in order to bring out two faint bands of asymptotic glider persistence. Shown below are selected larger-sample-size (10^5 samples) slices at constant t (b) and constant p (c).

Thus, gliders arise quite robustly from random initial conditions and proliferate for hundreds of time steps before slowly falling to extinction (except for two small ranges of p , for which gliders persist indefinitely). These results set an agenda for the analysis to be performed in the rest of this article. What are the processes by which gliders are created and destroyed? Can we quantify them? How does the balance between these processes change over time? How does it vary with p ? How does the interplay between creation and destruction give rise to all of the features described above? In order to answer such questions, we will first need to develop the necessary theoretical tools.

4 A Statistical Mechanics of Gliders

Let $\bar{g}_t(p)$ be the mean density of gliders in the grid at time t , given a random initial state characterized by a 1-probability p . When advancing in time, existing gliders can either persist or be destroyed and new gliders can be created. Let $\bar{\mathbf{G}}_t^+(p)$, $\bar{\mathbf{G}}_t^0(p)$, and $\bar{\mathbf{G}}_t^-(p)$ denote the corresponding mean glider density creation, persistence, and destruction operators, respectively. Then the mean glider density at time t can be expressed as

$$\begin{aligned}\bar{g}_t(p) &= \bar{g}_{t-1}(p) + \bar{\mathbf{G}}_{t-1}^+(p) - \bar{\mathbf{G}}_{t-1}^-(p) \\ &= \bar{\mathbf{G}}_{t-1}^0(p) + \bar{\mathbf{G}}_{t-1}^+(p).\end{aligned}$$

Note that the definitions of creation, persistence, and destruction are grounded in our previous analysis of what it means for a glider to persist [5]. Specifically, a glider at time t is considered to be the same as a glider at time $t + 1$ if the latter falls entirely within the light cone of the former.

Calculating these operators is an exercise in combinatorics (see the Appendix for full details). Let $\mathcal{G}_{5 \times 5}$ and $\mathcal{G}_{7 \times 7}$ respectively denote the sets of 5×5 and 7×7 configurations that contain a glider. Let $\mathcal{B}^1(\mathcal{G}_{5 \times 5})$ be the 1-basin of a glider, that is, the set of 7×7 configurations that evolve into 5×5 configurations containing a glider in one step. In addition, let $\mathcal{B}^1(\mathcal{G}_{5 \times 5}) \setminus \mathcal{G}_{7 \times 7}$ be the set of 7×7 configurations that are 1-precursors of gliders but that do not themselves contain a glider, and denote its cardinality by $|\mathcal{B}^1(\mathcal{G}_{5 \times 5}) \setminus \mathcal{G}_{7 \times 7}|$. Finally, let $|\mathcal{B}^1(\mathcal{G}_{5 \times 5}) \setminus \mathcal{G}_{7 \times 7}|_k$ denote the Hamming weight decomposition of $|\mathcal{B}^1(\mathcal{G}_{5 \times 5}) \setminus \mathcal{G}_{7 \times 7}|$, that is, the number of configurations in $\mathcal{B}^1(\mathcal{G}_{5 \times 5}) \setminus \mathcal{G}_{7 \times 7}$ that contain exactly k 1s.

With these definitions in place, the creation operator $\bar{\mathbf{G}}_0^+(p)$ can be expressed as just the expected increase in mean glider density due to glider precursors in the 1-basin evolving into gliders in the next step. Since setting each site to 1 with probability p in a $7 \times 7 = 49$ site grid induces a binomial distribution over the number of 1s in the grid, we have

$$\bar{\mathbf{G}}_0^+(p) = \mathbb{E} \left[\frac{|\mathcal{B}^1(\mathcal{G}_{5 \times 5}) \setminus \mathcal{G}_{7 \times 7}|_k}{\binom{49}{k}} \right], \quad k \sim B(49, p).$$

Expanding this expectation using the probability mass function of the binomial distribution $\binom{N}{k} p^k (1-p)^{N-k}$ and canceling the normalization factor, we obtain

$$\bar{\mathbf{G}}_0^+(p) = \sum_{k=0}^{49} |\mathcal{B}^1(\mathcal{G}_{5 \times 5}) \setminus \mathcal{G}_{7 \times 7}|_k p^k (1-p)^{49-k}.$$

A similar approach can be taken with the persistence operator $\bar{\mathbf{G}}_0^0(p)$, except that now our concern is with the subset of $\mathcal{B}^1(\mathcal{G}_{5 \times 5})$ that contains preexisting gliders. If we denote by $\tilde{\mathcal{G}}_{7 \times 7}$ the set of 7×7 configurations that do *not* contain a glider, then

$$\bar{\mathbf{G}}_0^0(p) = \sum_{k=0}^{49} |\mathcal{B}^1(\mathcal{G}_{5 \times 5}) \setminus \tilde{\mathcal{G}}_{7 \times 7}|_k p^k (1-p)^{49-k}.$$

Finally, the destruction operator $\bar{\mathbf{G}}_0^-(p)$ concerns the subset of glider-containing 7×7 configurations that evolve into 5×5 configurations without gliders. This is most easily computed from the persistence operator as

$$\bar{\mathbf{G}}_0^-(p) = \bar{g}_0(p) - \bar{\mathbf{G}}_0^0(p).$$

If we generalize the glider 1-basin $\mathcal{B}^1(\mathcal{G}_{5 \times 5})$ to the t -basin $\mathcal{B}^t(\mathcal{G})$ (the set of configurations that evolve to \mathcal{G} in t steps), then it is straightforward to express the glider density operators for arbitrary time:

$$\begin{aligned} \bar{\mathbf{G}}_t^+(p) &= \sum_{k=0}^{(2t+5)^2} |\mathcal{B}^{t+1}(\mathcal{G}_{5 \times 5}) \setminus \mathcal{B}^t(\mathcal{G}_{7 \times 7})|_k p^k (1-p)^{(2t+5)^2-k}, \\ \bar{\mathbf{G}}_t^0(p) &= \sum_{k=0}^{(2t+5)^2} |\mathcal{B}^{t+1}(\mathcal{G}_{5 \times 5}) \setminus \tilde{\mathcal{B}}^t(\mathcal{G}_{7 \times 7})|_k p^k (1-p)^{(2t+5)^2-k}, \\ \bar{\mathbf{G}}_t^-(p) &= \bar{g}_t(p) - \bar{\mathbf{G}}_t^0(p). \end{aligned}$$

For example, the basic idea of the generalized creation density operator expression is to remove from the $(t+1)$ -basin of a glider those configurations that would evolve to a glider in t steps. Note that these expressions assume that the size of the grid is large relative to $(2t+5) \times (2t+5)$. Once the two sizes become comparable, the boundary conditions of the grid must be taken into account.

Several different methods for computing the coefficients in these expressions are possible. Consider the creation operator coefficients $|\mathcal{B}^1(\mathcal{G}_{5 \times 5}) \setminus \mathcal{G}_{7 \times 7}|_k$. In the *forward algorithm*, we scan each possible 7×7 configuration, filter out those in $\mathcal{G}_{7 \times 7}$, and then evolve it one step forward in time and truncate to 5×5 . If the resulting configuration contains a glider, then we increment the coefficient corresponding to the number of 1s in the original 7×7 precursor. In the *backward algorithm*, we work backward from each 5×5 glider configuration, doing a depth-first search through possible inversions of the constituent cells and then filtering and counting as before. The *incremental aggregation algorithm*, which avoids individually visiting each possible precursor, can be used to calculate mean glider density operator coefficients in a way similar to its use for calculating GoL mean-field-theory coefficients [7]. Finally, considerable success has been achieved applying Boolean satisfiability solvers to a variety of problems in GoL [17, 21]. Details of the approach we take in this article to calculate glider density operator coefficients are given in the Appendix.

Plots of the $t = 1$ coefficients are shown in Figure 4. Note that the creation, persistence, and destruction coefficients have very different magnitudes and peak at different values of k . Unfortunately, the density operator coefficients quickly become very expensive to compute exactly. Indeed, the total glider 1-basin $\mathcal{B}^1(\mathcal{G}_{5 \times 5})$ already contains over 40 billion configurations. Thus, we will resort to Monte Carlo estimates of glider density and density operators for larger t .

5 Glider Origin and Proliferation

Using the above theory, we will analyze the time evolution of gliders in two stages (Figure 5). During stage 1, which will be the focus of this section, the glider density quickly rises to its peak. The following

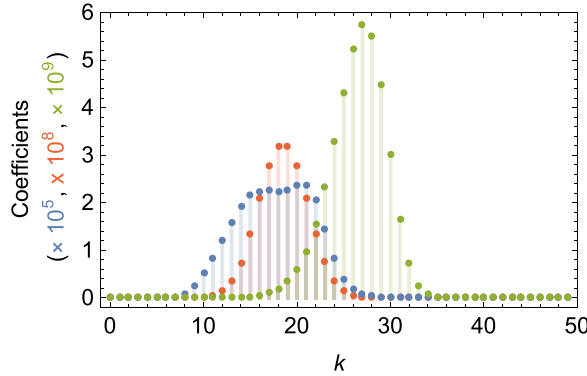


Figure 4. Glider creation $\bar{G}_0^+(p)$ (green), persistence $\bar{G}_0^0(p)$ (blue), and destruction $\bar{G}_0^-(p)$ (red) operator coefficients. Note that each set of coefficients has a different scale (indicated on the left).

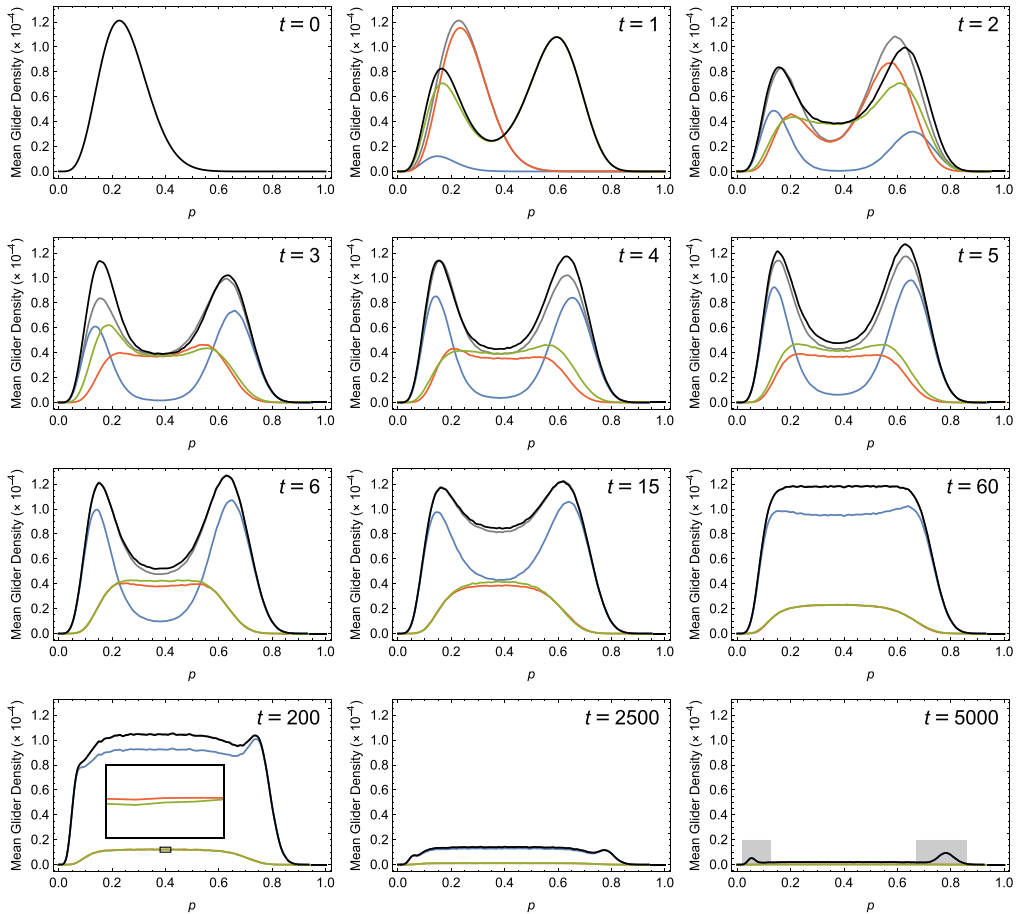


Figure 5. A decomposition of the mean glider density over p at selected times on a 100×100 grid. In each plot, the current mean glider density $\bar{g}_t(p)$ is black, the previous mean glider density $\bar{g}_{t-1}(p)$ is gray, and the mean creation $\bar{G}_{t-1}^+(p)$, persistence $\bar{G}_{t-1}^0(p)$, and destruction $\bar{G}_{t-1}^-(p)$ densities are green, blue, and red, respectively. The inset of the $t = 200$ plot shows an expanded view of the boxed area. The gray boxes in the $t = 5000$ plot mark the GoL asymptotic l-density transition regions shown in Figure 2. The $t = 0$ and $t = 1$ plots were calculated exactly, whereas the remaining plots were based on Monte Carlo estimates (10^5 samples per value of p).

section will study stage 2, during which the glider density slowly falls to its asymptotic value. The boundary between the two stages is somewhat p -dependent, but occurs at roughly $t \approx 60$. The analysis in these two sections decomposes and explains the family of plots in Figure 3(b).

The following relations are all trivial consequences of the definitions above, but can be useful for interpreting the correspondingly colored plots in Figure 5:

$$\begin{aligned}\bar{g}_t(p) &= \bar{\mathbf{G}}_{t-1}^0(p) + \bar{\mathbf{G}}_{t-1}^+(p), \\ \bar{g}_{t-1}(p) &= \bar{\mathbf{G}}_{t-1}^0(p) + \bar{\mathbf{G}}_{t-1}^-(p), \\ \bar{g}_t(p) - \bar{g}_{t-1}(p) &= \bar{\mathbf{G}}_{t-1}^+(p) - \bar{\mathbf{G}}_{t-1}^-(p).\end{aligned}$$

Our story begins on a random grid with 1-probability p . What is the density of gliders occurring completely by chance in a such a grid, before any time evolution has taken place? This density is given by $\bar{g}_0(p)$. Since there are 16 possible glider configurations and each glider contains five 1-cells and seventeen 0-cells, we have $\bar{g}_0(p) = 16p^5(1-p)^{17}$ (Figure 5, $t = 0$). This function has a single maximum at $p^* = 5/22 \approx 0.23$, where the density of the grid coincides with that of a glider and the probability of gliders occurring randomly is thus maximized. As we move away from this value, the chances of randomly creating a glider fall smoothly to zero.

Advancing one time step, the processes of glider creation, persistence, and destruction begin. The mean glider density at $t = 1$, $\bar{g}_1(p)$ (black curve in Figure 5, $t = 1$), now has two peaks. What causes these peaks? One might suspect that the left one is a holdover from the previous peak in $\bar{g}_0(p)$, but this turns out to be incorrect. Almost all random initial gliders are immediately destroyed by under-going destructive interactions with their environment (red curve). Only a small fraction of them persist (blue curve), and they do so at a smaller value of p than the earlier peak. In fact, almost all of the glider density observed at $t = 1$ is due to the creation of new gliders (green curve).

Comparing the green creation density plot for $t = 1$ in Figure 5 with the green creation coefficient plot in Figure 4 from which it is derived, we note an apparent discrepancy. Although $\bar{\mathbf{G}}_0^+(p)$ has two peaks, $|\mathcal{B} \setminus \mathcal{G}_{7 \times 7}|_k$ appears to have only one. Where does the second peak come from? Given the scale of the coefficient plot, it may seem as if the creation coefficients are zero below about $k = 15$, but in fact they are nonzero until $k = 4$. For example, the $k = 10$ creation coefficient is 509,208. These coefficients are differentially multiplied by the polynomial terms from the probability mass function of the binomial distribution, resulting in nonlinear amplification or attenuation at different values of p . Thus, the overall shape of operator density curves can only be understood in terms of the interaction between the coefficient and polynomial factors.

As time continues to advance, the interplay between creation and destruction becomes more complicated before eventually settling down to a simpler pattern that carries the mean glider density to its maximum around $t \approx 60$. At $t = 2$, the balance between creation and destruction at smaller p holds the left peak relatively constant, but the dominance of destruction at larger p pulls the right peak down and moves it to the right. Over the next several time steps, this balance shifts back and forth, alternately raising each peak until, by $t = 6$, both have reached their maximum height. Then the two peaks drop slightly and stabilize. Simultaneously, the valley between the two peaks begins to rise.

For the remainder of stage 1, changes in mean glider density occur only for values of p that fall within the valley between the two peaks. The floor of this valley slowly rises to become a mesa by the end of stage 1. The rise is fueled by a slight dominance of creation over destruction that can be seen clearly in the $t = 15$ plot. As the glider density approaches its maximum around $t \approx 60$, the magnitude of this creation bias steadily drops until creation and destruction temporarily balance and change in glider density pauses.

6 Glider Extinction and Asymptotics

Beyond the maximum glider density at $t \approx 60$, stage 2 begins. This stage is mainly characterized by a long slow collapse of the mesa observed at the end of stage 1. The drop in glider density is driven by

the dominance of destruction over creation in stage 2. The fall is slow because the imbalance is very small, as can be seen in the zoomed inset at $t = 200$, and it only decreases further as time passes.

During the collapse of the mesa, there is also quite a bit of transient activity around its edges. Initially, the mesa widens. Then its edges rise and flatten several times (e.g., Figure 5, $t = 200$). As the mesa continues to drop, the earlier valley eventually reappears (Figure 5, $t = 2500$). The bottom of the valley then slowly falls toward zero density as both creation and destruction cease. Asymptotically, only two small peaks of glider density at the edges of the former mesa or valley remain (Figure 5, $t = 5000$).

What is so special about these edges? Why do these narrow ranges of p values behave so differently, both transiently and asymptotically, from all of the others? At least part of the answer can be found in the statistical physics of the GoL universe. Recall that transition regions separate values of p for which $\bar{\rho}_\infty(p) = 0$ and $\bar{\rho}_\infty(p) = 0.029$ (gray boxes in Figure 2(b)). If we superimpose the locations of these transition regions in asymptotic 1-density on the plot of the asymptotic glider density $\bar{g}_\infty(p)$, the connection becomes clear (gray boxes in Figure 5, $t = 5000$). The transition regions in asymptotic 1-density align with the asymptotic glider density peaks, and thus with the peaks in the early parts of stage 1 and the mesa edges in stage 2.

What appears to be happening is the following. On the one hand, as in any nontrivial pattern, the only environments in which gliders can come into being are those of intermediate density; extreme densities quickly decay to the all-0 quiescent state. On the other hand, the only environments that gliders can survive in the long term are those that are fairly sparse; denser environments quickly lead to destructive interactions. The transition regions represent a tradeoff between these two extremes. Note that the asymptotic glider density peaks are shifted toward the outer edges of the 1-density transition regions, suggesting that the balance is not a trivial one.

Finally, in order to highlight the trends in glider density dynamics, it is useful to decompose it over time at a fixed value of p rather than as a function of p at fixed times as in Figure 5. This amounts to decomposing plots such as the one shown in Figure 3(c). Such a decomposition is shown in Figure 6 for $p = 0.4$ and $t \leq 100$. We see that, after a brief initial transient, all five curves climb to their peaks before slowly falling toward 0. Creation peaks first (green), followed quickly by destruction (red) and then later by $\bar{g}_{t-1}(p)$ (gray) and $\bar{g}_t(p)$ (black), and finally by persistence (blue). Note that, although creation dominates destruction at first, they quickly become almost perfectly balanced, so that extremely small differences between the two processes drive first the proliferation and eventually the extinction of gliders. Indeed, the two curves are almost tangent at their crossing point, so that the actual peak of glider density is quite subtle.

7 Refinements and Extensions

Applying the same general approach described above, we can also calculate more refined properties of the time evolution of gliders. We briefly consider two examples here.

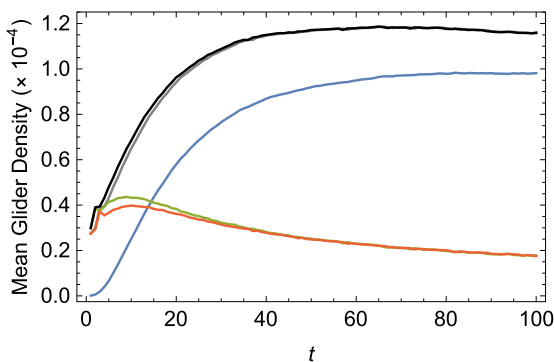


Figure 6. A decomposition of the mean glider density over time for $p = 0.4$. Color conventions are the same as in Figure 5. The curves represent means of 10^5 samples.

The first refinement we will examine is decomposing creation density by glider form. Consider $\bar{\mathbf{G}}_0^+(p)$ (green curve in the $t = 1$ plot in Figure 5). In order to split this into its wedge and rocket components (Figure 1), we need to separate the $|\mathcal{B}^1(\mathcal{G}_{5 \times 5}) \setminus \mathcal{G}_{7 \times 7}|_k$ coefficients into wedge and rocket contributions. The result is shown in Figure 7(a). Interestingly, we find that the rocket form dominates creation at lower values of p and the wedge form dominates at higher values. This is due to the fact that the rocket 1-basin is larger around the left peak and the wedge 1-basin is larger around the right peak. Decomposition by glider form can easily be applied to the other glider density operators to examine how the contribution of glider form varies with time.

A second possible refinement is to decompose the persistence density by perturbation class. Consider $\bar{\mathbf{G}}_0^0(p)$ (blue curve in the $t = 1$ plot in Figure 5). We know from previous work that the set of nondestructive glider perturbations can be divided into six classes depending on the state of the glider after the perturbation occurs [5]. These classes were assigned the arbitrary color names GRAY, BLACK, BLUE, BROWN, ORANGE, and GREEN. Of the gliders that persist from $t = 0$ to $t = 1$, what fraction arises from each class? Splitting the coefficients $|\mathcal{B}^1(\mathcal{G}_{5 \times 5}) \setminus \tilde{\mathcal{G}}_{7 \times 7}|_k$ by perturbation class, we can calculate the contributions from each class. The result is shown in Figure 7(b). We see that this persistence is dominated by the so-called null perturbations (GRAY and BLACK), which have no effect on the natural time evolution of rockets and wedges, respectively [5]. Although their peak contribution is almost two orders of magnitude smaller, BLUE perturbations begin to dominate for $p > 0.45$. BROWN, ORANGE, and GREEN perturbations are extremely small for all p . Once again, this decomposition can be extended to later times.

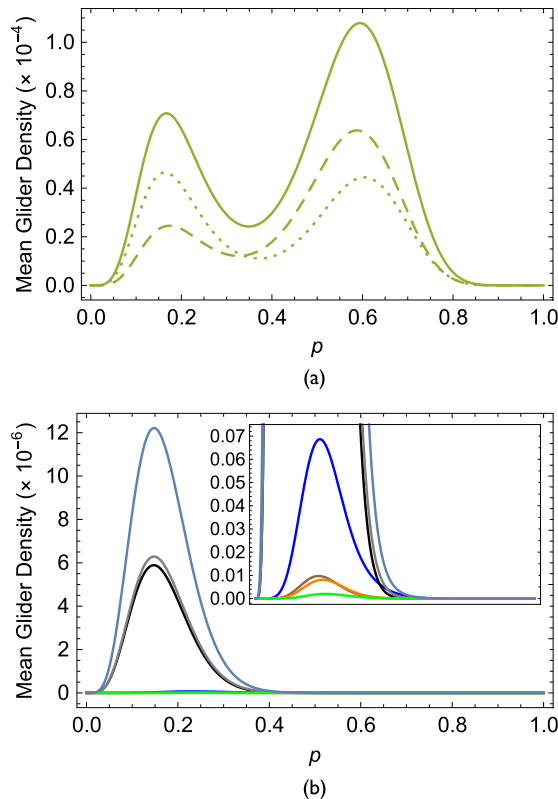
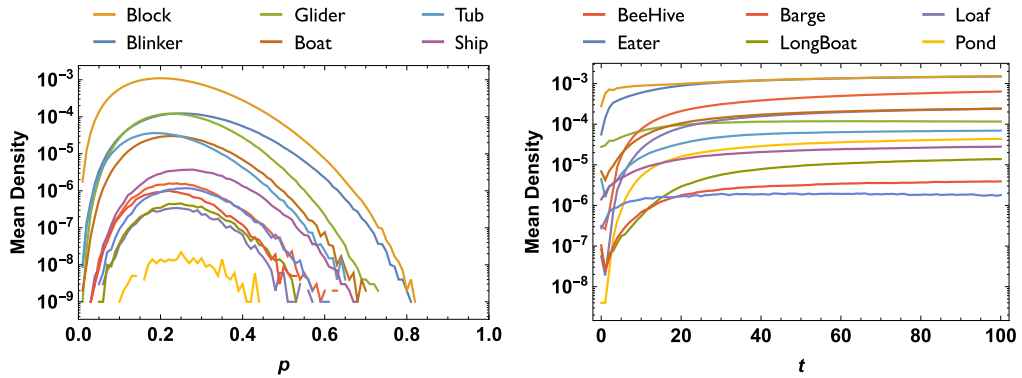
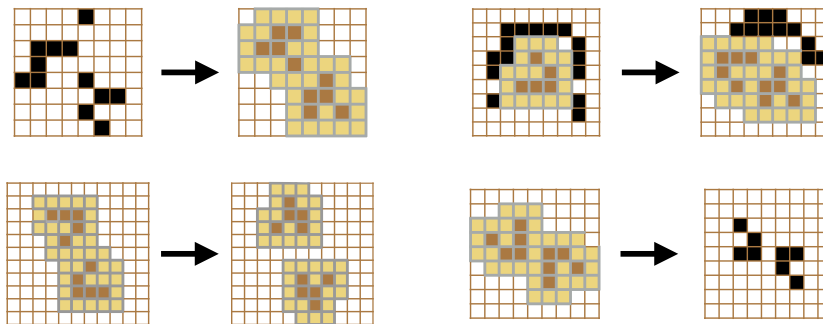


Figure 7. More refined decompositions of glider density operators. (a) A decomposition of glider creation $\bar{\mathbf{G}}_0^+(p)$ (solid curve) into its wedge (dashed) and rocket (dotted) contributions. (b) A decomposition of glider persistence $\bar{\mathbf{G}}_0^0(p)$ (upper blue curve) into its perturbation class contributions (GRAY, BLACK, BLUE, BROWN, ORANGE, and GREEN). The inset shows a vertical expansion of the plot. All of the curves in these plots result from exact calculations.

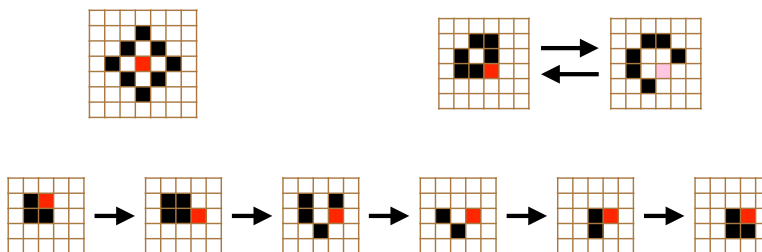
Finally, I present preliminary results from three extensions of the present work, each of which is mentioned in the discussion section. The first extension involves moving beyond a focus on gliders alone. As an initial step toward a broader analysis of the origin of autopoiesis in GoL, Figure 8(a) shows a statistical study of a dozen of the most common persistent bounded entities in GoL [9]. At left, the



(a)



(b)



(c)

Figure 8. Preliminary results from several extensions of the present work. (a) Mean density of twelve of the most common patterns in GoL for random initial grids with a 1-probability of p (left) and over time from an initially random grid with 1-probability $p = 0.4$ (right). Data represent the mean of 10^5 samples on a 100×100 grid with periodic boundary conditions. Images of these and many other GoL patterns can be found at <http://www.conwaylife.com/wiki>. (b) Examples of the ways in which an overlapping pair of gliders can be created from nonglider configurations (top left), split from an existing glider (top right), persist over time (bottom left), and annihilate one another (bottom right). (c) Examples of new persistent bounded entities that are stabilized by a single cell externally held on (red) or off (pink), including a static configuration (top left), an oscillating configuration (top right), and a moving configuration (bottom).

mean density of each class of entity in random grids with a 1-probability of p is shown. Note that one entity (Blinker) dominates all the others. Note also that the densities of all twelve entities peak over roughly the same range of p . At right, the initial time evolution of these densities is shown for $p = 0.4$. Note that the initial density of an entity is not necessarily predictive of its subsequent time evolution. For example, the entity with the lowest initial density (Pond) eventually surpasses four others whose densities were initially much higher. It is also interesting that two pairs of entities with very different initial densities evolve to almost the same density (Block + Blinker and Loaf + Boat).

The second extension concerns multiple gliders. The theory developed in this article accounts for the independent creation, persistence, and destruction of *individual* gliders. However, multiple gliders that share portions of their boundaries can also occur (Figure 8(b)). For example, overlapping glider pairs can appear spontaneously from nonglider precursors (Figure 8(b), top left), split from a single glider precursor (top right), persist from one time step to the next (bottom left), or destroy one another (bottom right). It would be interesting to extend the theory developed in this article to explicitly account for such multiglider interactions. For example, one could imagine defining a splitting operator for characterizing the mean glider density changes induced by one glider dividing into two.

The third extension concerns the nature of the Conway physics. In GoL, entities can persist indefinitely in an otherwise empty grid. In a more realistic physics, autopoietic systems would require non-equilibrium conditions supported by a flow of low-entropy energy and material. As a first step toward such nonequilibrium conditions, we can consider a version of GoL in which particular cells are held off or on in particular patterns. Under such driven conditions, new GoL entities can appear that feed off this external source of order. Three examples are shown in Figure 8(c). In the first (top left), a new static pattern that would collapse in standard GoL is stabilized by a single cell that is externally held on (red cell). In the second (top right), a new oscillating pattern is driven by alternately switching a single cell on (red) and off (pink). In the third example (bottom), a standard GoL block follows an externally held cell (red) that moves diagonally by one grid location every fifth time step.

8 Discussion

Employing a glider in the Game of Life as a toy model of autopoiesis, this article has taken some initial steps toward an investigation into the origin and proliferation of life from an autopoietic perspective. First, I presented the results of a large simulation experiment examining how the density of gliders evolves over time from random initial conditions parameterized by initial 1-density. Then I developed a glider statistical mechanics grounded in the dynamics of glider configurations and the combinatorics of their basins of attraction. This theory was then used to calculate the probability of gliders appearing in random grids and to decompose the time evolution of glider density into its creation, persistence, and destruction components. Finally, I showed how this theory could be extended to calculate more refined properties such as decomposing creation by glider form and persistence by perturbation class.

What can we conclude about the origin of gliders from this analysis? The glider era is certainly a well-delineated region in time and initial 1-density, suggesting that statistically robust processes are at work. However, this analysis has revealed a remarkably rich and, at times, rather delicate interplay between the processes of glider creation, persistence, and destruction underlying this era. Given this extended interplay, is it even correct to ask about *the* origin of gliders, as if it were a unique event? Although we can exactly calculate the probability that gliders appear in random grids, we saw that almost all such gliders are immediately destroyed and it is gliders that are subsequently created that fuel the proliferation. Perhaps we should focus instead on the overall dynamics of the underlying processes, with a particular emphasis on the conditions in which glider creation and persistence dominate glider destruction.

Because these processes are highly density-dependent, it is difficult to separate their dynamics from the broader statistical evolution of the GoL universe itself. This has an interesting resonance with the perspective put forward in a recent book [29]. The authors argue that the origin of life

involves not some isolated local event, but rather a series of planetary phase transitions in which the emergence of structure at one stage provides the foundation for the emergence of the next. Although highly simplified, GoL might be a useful toy model in which to investigate in some detail how such a global scenario might play out. For example, the analysis carried out for gliders in this article could easily be repeated for the dozen or so most common forms of persistent localized entities that typically arise from random initial conditions over roughly the same time scale in GoL. It would be interesting to study the co-emergence of this “ecosystem” as a collective phenomenon in the time evolution of GoL, toward which the preliminary work shown in Figure 8(a) is a first step.

In the short term, there are several other avenues for future work. There is still much to be done in fully understanding how the delicate interplay between the density operators and their various decompositions gives rise to all of the observed features of glider density evolution. This would be facilitated by improved algorithms for computing density operator coefficients, as well as better mathematical formulations. Finally, how might reproduction fit into this picture? Although nothing like a genome is present in a glider, a small number of “splitting” perturbations exist that produce two gliders from one, with the properties of the new gliders depending in a systematic way on the properties of the original one (Figure 8(c), top right).

More broadly, investigations into the origin of life have typically focused on specific prebiotic chemical interactions that could lead to a form of replication, metabolism, or compartmentalization [26]. Autopoiesis can be thought of as providing a kind of organizational backbone for the molecular and energetic considerations of operating in the physical world, as every living system must do. Perhaps the most interesting implication of adopting an autopoietic perspective on questions of origins is the shift it induces to what might be called an “organization-first” approach. The basic idea is to change the focus from specific molecular components and reaction pathways to the simplest possible autopoietic organizations relative to a given physics. Cellular automata offer a rich variety of simple physics in which we can investigate the emergence, degradation, stabilization, and complexification of organizations. However, carrying such a program forward will require moving beyond the kind of purely statistical treatment undertaken in this article to a direct investigation of the dynamics that underlie these configuration statistics. How do sets of interacting processes spontaneously organize into closed networks with a self-generated boundary? How are we to characterize the dynamics of process dependence networks themselves? Despite the fact that an understanding of the dynamics of organizations has barely begun, both in general [13, 14, 16] and for GoL specifically [6], this is the direction in which we must push.

Of course, the study of abstract toy models can only take us so far. Ultimately, it will be necessary to take the physical reality into account. The best way to conceive of these physical details is as a source of material constraint on the formation of autopoietic systems. Very simple autopoietic systems are common in GoL owing to its intrinsically dissipative (state space volumes contract onto limit sets) and therefore pattern-forming nature. In the physical world, much more work (both figuratively and literally) needs to be done to produce and maintain autopoietic organizations, significantly raising their minimal complexity. As is well known, properly harnessing energy flows is essential to the physical instantiation of autopoiesis, making nonequilibrium thermodynamics a central concern.

One possible path toward such physical concerns is to explore the application of autopoietic concepts to more realistic protocell models [2]. However, the path that I prefer is an incremental one, endowing simple cellular automata models such as GoL with increasingly more physically realistic characteristics. This way we can systematically explore how each additional physical constraint influences the networks of processes that can form. Because cellular automata have been seriously pursued as a modeling methodology for physical systems for many years, there is a wide literature to draw upon for this endeavor [11, 12, 32, 33]. For example, reversibility [24, 35], temperature dependence [1, 27], conserved quantities [10, 31], driven/nonequilibrium conditions (Figure 8(c)), and so on, can all be incorporated, and cellular automata have even been used to model various aspects of biochemistry [20]. In any case, we need to identify the simplest physical settings in which generic features of the origin of life can be explored so that we can place the specific historical contingencies

underlying the emergence of terrestrial life into its proper position within the broader space of possible scenarios by which autopoiesis more broadly can arise within an initially nonautopoietic universe.

Acknowledgments

I would like to thank Eran Agmon and the anonymous reviewers for their feedback on an earlier draft of this article. Portions of this work were presented at the workshop on “The Biological Foundations of Enactivism” held at the 2016 Artificial Life XV Conference in Cancún, Mexico, and I thank the participants for discussion. Computation performed for this research was supported in part by Lilly Endowment, Inc., through its support for the Indiana University Pervasive Technology Institute, and in part by the Indiana METACyt Initiative. The Indiana METACyt Initiative at IU is also supported in part by Lilly Endowment, Inc.

References

1. Adachi, S., Peper, F., & Lee, J. (2004). The Game of Life at finite temperature. *Physica D*, 198(3–4), 182–196.
2. Agmon, E., Gates, A. J., Churavy, V., & Beer, R. D. (2016). Exploring the space of viable configurations in a model of metabolism-boundary co-construction. *Artificial Life*, 22, 153–171.
3. Bagnoli, F., Rechtman, R., & Ruffo, S. (1991). Some facts of Life. *Physica A*, 171, 249–264.
4. Beer, R. D. (2004). Autopoiesis and cognition in the Game of Life. *Artificial Life*, 10, 309–326.
5. Beer, R. D. (2014). The cognitive domain of a glider in the Game of Life. *Artificial Life*, 20, 183–206.
6. Beer, R. D. (2015). Characterizing autopoiesis in the Game of Life. *Artificial Life*, 21, 1–19.
7. Beer, R. D. (2017). Computing aggregate properties of preimages for 2D cellular automata. *Chaos*, 27, 111104.
8. Beer, R. D. (2018). On the origin of gliders. In T. Ikegami, N. Virgo, O. Witkowski, M. Oka, R. Suzuki, & H. Iizuka (Eds.), *Proceedings of the 2018 Conference on Artificial Life* (pp. 67–74). Cambridge, MA: MIT Press.
9. Berlekamp, E. R., Conway, J. H., & Guy, R. K. (1982). What is Life? In E. R. Berlekamp, J. H. Conway, & R. K. Guy (Eds.), *Winning ways for your mathematical plays*, Vol. 2 (Chapter 25, pp. 817–850). New York: Academic Press.
10. Capobianco, S., & Toffoli, T. (2012). Conserved quantities in discrete dynamics: What can be recovered from Noether’s theorem, how, and why? *Natural Computing*, 11, 565–577.
11. Chopard, B., & Droz, M. (1998). *Cellular automata modeling of physical systems*. Cambridge, UK: Cambridge University Press.
12. Chopard, B. (2009). Cellular automata modeling of physical systems. In R. A. Meyers (Ed.), *Encyclopedia of complexity and systems science* (pp. 865–892). New York: Springer-Verlag.
13. Crutchfield, J. P., & Görnerup, O. (2006). Objects that make objects: The population dynamics of structural complexity. *Journal of the Royal Society Interface*, 3, 345–349.
14. Ditttrich, P., & Speroni di Fenizio, P. (2007). Chemical organisation theory. *Bulletin of Mathematical Biology*, 69, 1199–1231.
15. Dyson, F. (1999). *Origins of life*. Cambridge, UK: Cambridge University Press.
16. Fontanna, W., & Buss, L. W. (1994). The arrival of the fittest: Toward a theory of biological organization. *Bulletin of Mathematical Biology*, 56, 1–64.
17. Hartman, C., Heule, M. H., Kwekkeboom, K., & Noels, A. (2013). Symmetry in Gardens of Eden. *The Electronic Journal of Combinatorics*, 20(3), 16.
18. Joyce, G. F., & Orgel, L. E. (2006). Progress toward understanding the origin of the RNA world. In R. F. Gesteland (Ed.), *The RNA world* (3rd ed.), (pp. 23–56). Boca Raton, FL: CRC Press.
19. Kaufmann, S. A. (2000). *Investigations*. Oxford, UK: Oxford University Press.
20. Kier, L. B., & Seybold, P. G. (2009). Cellular automata modeling of complex biochemical systems. In R. A. Meyers (Ed.), *Encyclopedia of complexity and systems science* (pp. 848–865). New York: Springer-Verlag.
21. Knuth, D. E. (2015). *The art of computer programming, Vol. 4, Fascicle 6: Satisfiability*. Boston: Addison-Wesley.

22. Lanier, K. A., & Williams, L. D. (2017). The origin of life: Models and data. *Journal of Molecular Evolution*, 84, 85–92.
23. Luisi, P. L. (2006). *The emergence of life: From chemical origins to synthetic biology*. Cambridge, UK: Cambridge University Press.
24. Margolus, N. (1984). Physics-like models of computation. *Physica D*, 10, 81–95.
25. Maturana, H. R., & Varela, F. J. (1973/1980). Autopoiesis: The organization of the living. In H. R. Maturana & F. J. Varela (Eds.), *Autopoiesis and Cognition*. Dordrecht, The Netherlands: D. Reidel.
26. Ruiz-Mirazo, K., Briones, C., & de la Escosura, A. (2014). Prebiotic systems chemistry: New perspectives for the origins of life. *Chemical Reviews*, 114, 285–366.
27. Schulman, L. S., & Seiden, P. (1978). Statistical mechanics of a dynamical system based on Conway’s Game of Life. *Journal of Statistical Physics*, 19, 293–314.
28. Segré, D., Ben-Eli, D., Deamer, D. W., & Lancet, D. (2001). The lipid world. *Origins of Life and Evolution of the Biosphere*, 31, 119–145.
29. Smith, E., & Morowitz, H. J. (2016). *The origin and nature of life on earth: The emergence of the fourth geosphere*. Cambridge, UK: Cambridge University Press.
30. Szostak, J. W., Bartel, D. P., & Luisi, P. L. (2001). Synthesizing life. *Nature*, 409, 387–390.
31. Taati, S. (2012). Conservation laws in cellular automata. In G. Rozenberg, T. Bäck, & J. N. Kok. (Eds.), *Handbook of natural computing* (pp. 259–286). New York: Springer-Verlag.
32. Toffoli, T. (1984). Cellular automata as an alternative to (rather than an approximation of) differential equations in modeling physics. *Physica D*, 10(1–2), 117–127.
33. Toffoli, T., & Margolus, N. (1987). *Cellular automata machines: A new environment for modeling*. Cambridge, MA: MIT Press.
34. Varela, F. J. (1979). *Principles of biological autonomy*. New York: North-Holland.
35. Vichniac, G. Y. (1984). Simulating physics with cellular automata. *Physica D*, 10(1–2), 96–116.
36. Walker, S. I., Packard, N., & Cody, G. D. (2018). Re-conceptualizing the origins of life. *Philosophical Transactions of the Royal Society A*, 375, 20160337.

Appendix

This appendix gives the details underlying the calculation of the $t = 0$ glider density operator coefficients described in the main text. In principle, one could compute coefficients such as $|\mathcal{B}^1(\mathcal{G}_{5 \times 5}) \setminus \mathcal{G}_{7 \times 7}|_k$ by explicitly generating the set $\mathcal{B}^1(\mathcal{G}_{5 \times 5})$, removing all elements that contain gliders, and then counting the number of 1s in each remaining element. However, the sizes of these sets make such a direct approach untenable in practice. Instead, we directly compute the Hamming weight decompositions of only relatively small sets and then calculate the coefficients of interest by appropriately combining these “atomic” weights.

The basic idea of the calculation is illustrated in Figure 9. In radius-1 cellular automata such as GoL, the configuration of an $n \times n$ lattice at time t is influenced by the configuration of the enclosing $(n - 2) \times (n - 2)$ lattice at time $t - 1$. Let $\mathcal{L}_{n \times n}$ denote the set of all configurations of an $n \times n$ lattice, let $\mathcal{G}_{n \times n}$ denote the subset of $\mathcal{L}_{n \times n}$ that contains a glider, and let $\mathcal{B}^1(\mathcal{G}_{5 \times 5})$ denote the subset of $\mathcal{L}_{7 \times 7}$ that evolves to $\mathcal{G}_{5 \times 5}$ in one step (i.e., its 1-basin). Recall from the main text that, for any given subset of interest \mathcal{S} , we need to compute the Hamming weight decomposition $|\mathcal{S}|_k$ in order to compute $\bar{\mathbf{G}}_0^{\mathcal{S}}(p)$ from

$$\bar{\mathbf{G}}_0^{\mathcal{S}}(p) = \mathbb{E} \left[\frac{|\mathcal{S}|_k}{\binom{49}{k}} \right] = \sum_{k=0}^{49} |\mathcal{S}|_k p^k (1-p)^{49-k}.$$

For the persistence operator $\bar{\mathbf{G}}_0^0(p)$, the subset of interest is $\mathcal{B}^1(\mathcal{G}_{5 \times 5}) \setminus \tilde{\mathcal{G}}_{7 \times 7}$ (indicated in blue in Figure 9). This subset is composed of all the ways that a glider can persist from one time step to the next. Previous work demonstrated that there are exactly six ways that this can happen, arbitrarily

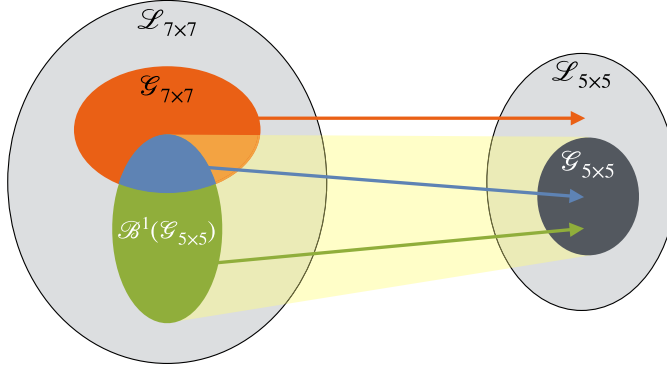


Figure 9. An illustration of the various subsets of configurations relevant for the calculations given in the Appendix. $\mathcal{L}_{n \times n}$ denotes the set of $n \times n$ lattices in GoL, $\mathcal{G}_{n \times n}$ denotes the subset of $n \times n$ lattices containing gliders, and $\mathcal{B}^1(\mathcal{G}_{5 \times 5})$ denotes the 1-basin of $\mathcal{G}_{5 \times 5}$ (that is, the set of 7×7 precursors of $\mathcal{G}_{5 \times 5}$). The subsets of $\mathcal{L}_{7 \times 7}$ related to glider creation, persistence, and destruction are colored green, blue, and red, respectively.

labeled by colors [4]. With W indicating the wedge form and R indicating the rocket form, we can write these possibilities as $W \xrightarrow{\text{BLACK}} R$, $W \xrightarrow{\text{BLUE}} W$, $W \xrightarrow{\text{BROWN}} R$, $W \xrightarrow{\text{ORANGE}} R$, $R \xrightarrow{\text{GRAY}} W$, and $R \xrightarrow{\text{GREEN}} R$. Then we have that the Hamming weight decompositions of the subset of gliders that persist to the wedge form and the subset of gliders that persist to the rocket form are given by

$$|G \rightarrow W|_k = \left| W \xrightarrow{\text{BLUE}} W \right|_k + \left| R \xrightarrow{\text{GRAY}} W \right|_k,$$

$$|G \rightarrow R|_k = \left| W \xrightarrow{\text{BLACK}} R \right|_k + \left| W \xrightarrow{\text{BROWN}} R \right|_k + \left| W \xrightarrow{\text{ORANGE}} R \right|_k + \left| R \xrightarrow{\text{GREEN}} R \right|_k,$$

respectively. From these we can compute the required persistence operator coefficients using

$$|\mathcal{B}^1(\mathcal{G}_{5 \times 5}) \setminus \tilde{\mathcal{G}}_{7 \times 7}|_k = |G \rightarrow W|_k + |G \rightarrow R|_k.$$

Finally, a term such as $\left| W \xrightarrow{\text{BROWN}} R \right|_k$ can be computed from the solutions of

$$f \left(\begin{pmatrix} x_1 & x_2 & x_3 & 0 & 0 & 0 & x_4 \\ x_5 & x_6 & 0 & 0 & 1 & 0 & x_7 \\ x_8 & x_9 & 0 & 1 & 0 & 0 & 0 \\ x_{10} & x_{11} & 0 & 1 & 1 & 1 & 0 \\ x_{12} & x_{13} & 0 & 0 & 0 & 0 & 0 \\ x_{14} & x_{15} & x_{16} & x_{17} & x_{18} & x_{19} & x_{20} \\ x_{21} & x_{22} & x_{23} & x_{24} & x_{25} & x_{26} & x_{27} \end{pmatrix} \right) = \begin{pmatrix} \cdot & 0 & 0 & 0 & \cdot \\ \cdot & 0 & 1 & 0 & 0 \\ 0 & 0 & 1 & 1 & 0 \\ 0 & 1 & 0 & 1 & 0 \\ 0 & 0 & 0 & 0 & 0 \end{pmatrix},$$

where f is the GoL update function and dots denote locations whose values are irrelevant. As mentioned in the main text, there are many different ways to solve such equations. For the computations underlying the results in this article, we extract a set of relations among the x_i from this equation, simplify them symbolically, and compile a specialized iterative solver that counts the number of solutions in each Hamming weight class without having to store those solutions. The resulting weights must then be multiplied by 8 to take account of the fact that the rocket form on the right-hand side of this equation can appear in four different orientations and two different chiralities. The other five terms can be computed in the same manner.

For the creation operator $\bar{\mathbf{G}}_0^+(p)$, the subset of interest is $\mathcal{B}^1(\mathcal{G}_{5 \times 5}) \setminus \mathcal{G}_{7 \times 7}$ (indicated in green in Figure 9). We can express this as

$$|\mathcal{B}^1(\mathcal{G}_{5 \times 5}) \setminus \mathcal{G}_{7 \times 7}|_{\kappa} = |\mathcal{B}^1(\mathcal{W}_{5 \times 5})|_{\kappa} + |\mathcal{B}^1(\mathcal{R}_{5 \times 5})|_{\kappa} - (|G \rightarrow W|_{\kappa} + |G \rightarrow R|_{\kappa}),$$

where $\mathcal{B}^1(\mathcal{W}_{5 \times 5})$ and $\mathcal{B}^1(\mathcal{R}_{5 \times 5})$ are the 7×7 configurations that evolve to wedges or rockets in 5×5 , respectively. For example, $|\mathcal{B}^1(\mathcal{W}_{5 \times 5})|_{\kappa}$ can be computed from solutions to

$$f \left(\begin{pmatrix} \mathfrak{x}_1 & \mathfrak{x}_2 & \mathfrak{x}_3 & \mathfrak{x}_4 & \mathfrak{x}_5 & \mathfrak{x}_6 & \mathfrak{x}_7 \\ \mathfrak{x}_8 & \mathfrak{x}_9 & \mathfrak{x}_{10} & \mathfrak{x}_{11} & \mathfrak{x}_{12} & \mathfrak{x}_{13} & \mathfrak{x}_{14} \\ \mathfrak{x}_{15} & \mathfrak{x}_{16} & \mathfrak{x}_{17} & \mathfrak{x}_{18} & \mathfrak{x}_{19} & \mathfrak{x}_{20} & \mathfrak{x}_{21} \\ \mathfrak{x}_{22} & \mathfrak{x}_{23} & \mathfrak{x}_{24} & \mathfrak{x}_{25} & \mathfrak{x}_{26} & \mathfrak{x}_{27} & \mathfrak{x}_{28} \\ \mathfrak{x}_{29} & \mathfrak{x}_{30} & \mathfrak{x}_{31} & \mathfrak{x}_{32} & \mathfrak{x}_{33} & \mathfrak{x}_{34} & \mathfrak{x}_{35} \\ \mathfrak{x}_{36} & \mathfrak{x}_{37} & \mathfrak{x}_{38} & \mathfrak{x}_{39} & \mathfrak{x}_{40} & \mathfrak{x}_{41} & \mathfrak{x}_{42} \\ \mathfrak{x}_{43} & \mathfrak{x}_{44} & \mathfrak{x}_{45} & \mathfrak{x}_{46} & \mathfrak{x}_{47} & \mathfrak{x}_{48} & \mathfrak{x}_{49} \end{pmatrix} \right) = \begin{pmatrix} \cdot & 0 & 0 & 0 & \cdot \\ \cdot & 0 & 1 & 0 & 0 \\ 0 & 0 & 0 & 1 & 0 \\ 0 & 1 & 1 & 1 & 0 \\ 0 & 0 & 0 & 0 & 0 \end{pmatrix}$$

and similarly for $|\mathcal{B}^1(\mathcal{R}_{5 \times 5})|_{\kappa}$. Once again, the resulting coefficients need to be multiplied by 8.

For the destruction operator $\bar{\mathbf{G}}_0^-(p)$, the subset of interest is $\mathcal{G}_{7 \times 7} \setminus \mathcal{B}^1(\mathcal{G}_{5 \times 5})$ (indicated in red in Figure 9). Since, as explained in the main text, the destruction operator can be written in terms of other known quantities, a direct calculation of the destruction operator coefficients is unnecessary. However, to derive the destruction coefficients plotted in Figure 4, we use

$$|\mathcal{G}_{7 \times 7} \setminus \mathcal{B}^1(\mathcal{G}_{5 \times 5})|_{\kappa} = |\mathcal{G}_{7 \times 7}|_{\kappa} - (|G' \rightarrow W'|_{\kappa} + |G' \rightarrow R'|_{\kappa}),$$

where the terms in the parentheses are calculated in the same way as the analogous unprimed terms above except that we use a past-centered formulation of the individual wedge and rocket transformation terms rather than the future-centered formulation employed above. For example, the equation from which the term $\left| W' \xrightarrow{\text{BROWN}} R' \right|$ is derived becomes

$$f \left(\begin{pmatrix} \mathfrak{x}_1 & \mathfrak{x}_2 & \mathfrak{x}_3 & \mathfrak{x}_4 & \mathfrak{x}_5 & \mathfrak{x}_6 & \mathfrak{x}_7 \\ \mathfrak{x}_8 & \mathfrak{x}_9 & 0 & 0 & 0 & \mathfrak{x}_{10} & \mathfrak{x}_{11} \\ \mathfrak{x}_{12} & \mathfrak{x}_{13} & 0 & 1 & 0 & 0 & \mathfrak{x}_{14} \\ \mathfrak{x}_{15} & 0 & 0 & 0 & 1 & 0 & \mathfrak{x}_{16} \\ \mathfrak{x}_{17} & 0 & 1 & 1 & 1 & 0 & \mathfrak{x}_{18} \\ \mathfrak{x}_{19} & 0 & 0 & 0 & 0 & 0 & \mathfrak{x}_{20} \\ \mathfrak{x}_{21} & \mathfrak{x}_{22} & \mathfrak{x}_{23} & \mathfrak{x}_{24} & \mathfrak{x}_{25} & \mathfrak{x}_{26} & \mathfrak{x}_{27} \end{pmatrix} \right) = \begin{pmatrix} \cdot & \cdot & \cdot & \cdot & \cdot & \cdot & \cdot \\ \cdot & \cdot & \cdot & \cdot & \cdot & \cdot & \cdot \\ \cdot & \cdot & \cdot & 0 & 0 & 0 & \cdot \\ \cdot & \cdot & 0 & 0 & 1 & 0 & \cdot \\ \cdot & \cdot & 0 & 1 & 1 & 0 & 0 \\ \cdot & \cdot & 0 & 1 & 0 & 1 & 0 \\ \cdot & \cdot & 0 & 0 & 0 & 0 & 0 \end{pmatrix},$$

and $|\mathcal{G}_{7 \times 7}|_{\kappa}$ is given by decomposing all the ways that a glider can be centered in a 7×7 lattice:

$$|\mathcal{G}_{7 \times 7}|_{\kappa} = \begin{cases} 16 \binom{27}{\kappa-5}, & 5 \leq \kappa \leq 32, \\ 0 & \text{otherwise.} \end{cases}$$

Finally, we have the plots in Figure 7. The coefficients of the wedge and rocket decompositions of $\bar{\mathbf{G}}_0^+(p)$ (Figure 7(a)) are given by $|\mathcal{B}^1(\mathcal{W}_{5 \times 5})|_{\kappa} - |G \rightarrow W|_{\kappa}$ and $|\mathcal{B}^1(\mathcal{W}_{5 \times 5})|_{\kappa} - |G \rightarrow R|_{\kappa}$, respectively. The perturbation class decomposition coefficients in Figure 7b are given by the six unprimed glider transformation terms $\left| W \xrightarrow{\text{BLACK}} R \right|_{\kappa}, \dots, \left| R \xrightarrow{\text{GRAY}} W \right|_{\kappa}$.